Effects of different design parameters on the stone-impact resistance of automotive windshields

X Sun* and M A Khaleel
Pacific Northwest National Laboratory, Richland, Washington, USA

The manuscript was received on 9 August 2004 and was accepted after revision for publication on 25 April 2005.

DOI: 10.1243/095440705X34784

Abstract: A constitutive model based on continuum damage mechanics is used to study the stone-impact resistance of automotive windshields. An axisymmetric finite element model is created to simulate the transient dynamic response and impact-induced damage tensors for laminated glass layers subject to stone-impact loading. The windshield glass consists of two glass outer layers laminated by a thin poly(vinyl butyral) (PVB) layer. The constitutive behaviour of the glass layers is simulated using the continuum damage mechanics model with linear damage evolution. The PVB layer is modelled with a linear viscoelastic solid. The model is used to predict and examine damage patterns on different glass surfaces for different windshield designs including variations in ply thickness and curvatures.

Keywords: automotive windshield design, stone impact, impact resistance, glass cracking, glass damage, star-shaped crack, web-shaped crack, Hertzian cone crack

1 INTRODUCTION

Weight reduction is a major challenge for all automotive manufacturers since it contributes significantly to fuel economy and compliance with government regulations. The 45–70 kg of glass in today's automobiles can potentially be reduced by using tempered thin glass, asymmetric glass construction, and glass–plastic bilayers. The development of these lightweight glazing products needs to address many structural and regulatory issues. These issues include windshield impact resistance, the glazing system's contribution to vehicle structural rigidity and thermal management, etc. Although the weight reduction of the glazing system itself can be limited, there may be a cascading effect on weight savings in other vehicle areas. For example, it may be possible to decrease weight in other vehicle parts owing to increased body stiffness imparted by the stronger and thinner glass. The contribution of improved thinner glass properties to enhancing thermal management may also make it possible to reduce weight in thermal management components. One of the key barriers to using thinner glazing is the lack of understanding of its structural behaviour as an integrated part of the vehicle and its resistance to the impact loading of a flying object.

The objective of this study is to predict the damage zone size and shape of an automotive windshield glass subject to the normal impact loading of a flying object. The automotive safety glass is constructed by placing an adhesive polymeric interlayer between two soda–lime glass plies. Poly(vinyl butyral) (PVB) is the industry standard interlayer because of its adhesive and optical qualities. The purpose of the interlayer is to prevent the glass plies from shattering on impact, thereby greatly reducing the possibility of body injury caused by sharp pieces of flying glass.

There is a vast amount of literature on the static indentation stress fields, cracking, and fracture in brittle materials such as glass and ceramic (see, for example, the review article on this topic in reference [1]). A diversity of cracks may be generated in semi-infinite glass media by static indentation contact. Experimental observations indicate that there are five major crack types: cone cracks, radial cracks, median vent cracks, half-penny cracks, and lateral cracks. Comprehensive reviews of glass indentation cracking and the crack morphology associated with

* *Corresponding author: Pacific Northwest National Laboratory, K1-85, 906 Battelle Blvd, Richland, WA 99352, USA. email: xin.sun@pnl.gov*

each type of crack can be found in the literature [2–4]. However, previous studies on impact resistance of thin glass plies are very limited. Among them, Flocker and Dharani [5, 6] used finite element analyses to study the effects of a Hertzian cone crack on the impact resistance of a laminated window in a civil engineering application. A very fine mesh and a large number of elements were used to study the effect of one damage mechanism, namely the Hertzian cone, and no other discrete or volumetric damage mechanisms were considered. In addition, the inclination angle and propagation velocity of the Hertzian cone crack were pre-assumed on the basis of some empirical formulations [5, 6].

Since the actual damage patterns of thin laminated glass subject to impact loading are a combination of different damage mechanisms, the continuum damage mechanics (CDM) model developed by Sun and Khaleel [7] presents a feasible approach in studying the different windshield damage patterns subject to the impact loading of flying objects.

Recently, Sun *et al.* [8] used the above CDM-based constitutive model in studying the impact resistance of monolithic glass subject to impact loading. The analysis procedures and the constitutive model were validated by comparing the predicted strain histories of the glass ply with experimental strain gauge measurements. In addition, the damage parameters in the constitutive model were established and calibrated under impact loading conditions using experimental observations from stair-stepping impact tests.

In this study, the same CDM model and damage parameters as described above are employed to study the effects of different windshield design parameters, i.e. the thickness of the inner and outer glass ply, and windshield curvatures on its stone-impact resistance. Explicit finite element analyses are used to simulate the impact event, and the final size and shape of the damage zone are determined by interpreting different components of the damage tensor [7, 8].

2 MODEL DESCRIPTION AND MATERIAL CONSTITUTIVE BEHAVIOURS

First, a steel ball with a 3 mm radius and a specified initial velocity is set to impact with the laminated glass layers (Fig. 1). Normal impact is treated only. The glass and PVB layers in the laminated windshield are modelled with four-node bilinear axisymmetric elements. Different surface numbers for the two glass layers are labelled in Fig. 1 for easy identification. Perfect bonding between the glass and the PVB layer is assumed since delamination is not usually observed in the cracked windshield. The commercial finite element code ABAQUS EXPLICIT [9] is used with automatic time incrementation, and contact surfaces are set up between the indenter surface and surface 1 of the glass layers to prevent inner penetration. The diameter of the total windshield area considered in this study is 60 mm. Since the

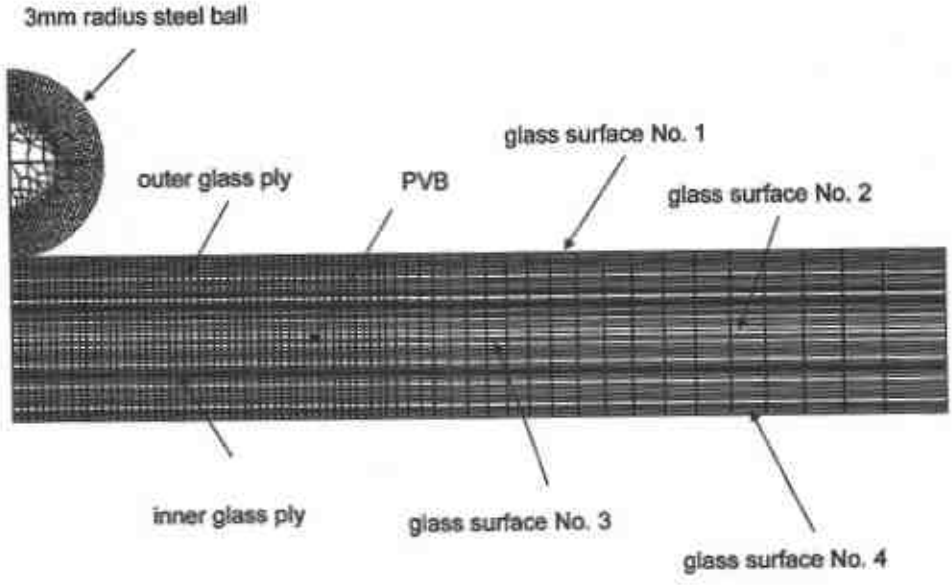

Fig. 1 The laminated glass ply impact model

radius of the indenter is much smaller than the in-plane dimension of the windshield, infinite four-node axisymmetric elements are used around the perimeter of the model.

The non-linearity of glass resulting from the deformation process is modelled by introducing an anisotropic damage tensor D_{ij} into the constitutive equation [7, 8]. The constitutive relationship of the material is expressed in the form

$$\sigma_{ij} = ([K^{\mathrm{u}}_{ijkl}] + [K^{\mathrm{d}}_{ijkl}])\{\varepsilon_{kl}\} \tag{1}$$

in which the stiffness matrix is divided into two matrices $[K^{\mathrm{u}}_{ijkl}]$ and $[K^{\mathrm{d}}_{ijkl}]$, which denote the stiffness matrix for the undamaged material and for the added influence of damage respectively. The full expressions of these matrix components are given as

$$K^{\mathrm{u}}_{ijkl} = \lambda\delta_{ij}\delta_{kl} + \mu(\delta_{ik}\delta_{jl} + \delta_{il}\delta_{kj}) \tag{2}$$

$$K^{\mathrm{d}}_{ijkl} = C_1(\delta_{ij}D_{kl} + \delta_{kl}D_{ij}) + C_2(\delta_{jk}D_{il} + \delta_{il}D_{jk}) \tag{3}$$

where λ and μ are the Lamé constants for glass given by

$$\lambda = \frac{E\nu}{(1+\nu)(1-2\nu)}, \qquad \mu = \frac{E}{2(1+\nu)}$$

in which Young's modulus E of glass is 72 GPa and Poisson's ratio ν is 0.25. The damage parameters C_1 and C_2 are determined such that the axial stress equals zero when the damage component D_{11} approaches 1.0 for a uniaxial tension test according to equations (1) to (3). Using Young's modulus and Poisson's ratio for glass, we determine that $C_1 = 28.9$ GPa and $C_2 = -43.44$ GPa.

The damage tensor was determined by a damage evolution law [7, 8] in which two basic modes of damage are considered analogous to the fracture mechanics definition:

(a) damage caused by principal normal stress components which manifests as an opening mode of failure (i.e. mode I);
(b) damage caused by maximum shear stress components (i.e. mode II).

The damage components due to normal principal stresses are assumed to follow a simple linear damage evolution law in which the opening mode damage is linearly related to the corresponding tensile principal stress component in a certain stress range above the threshold value according to

$$D_{ii} = \begin{cases} 0, & \sigma_i \leqslant \sigma_{\mathrm{threshold}} \\ \dfrac{\sigma_i - \sigma_{\mathrm{threshold}}}{\sigma_{\mathrm{crit}} - \sigma_{\mathrm{threshold}}}, & \sigma_{\mathrm{threshold}} < \sigma_i < \sigma_{\mathrm{crit}}, \quad i = 1, 2, 3 \\ 1, & \sigma_i \geqslant \sigma_{\mathrm{crit}} \end{cases} \tag{4}$$

The damage caused by the maximum shear stress components in the ij plane is assumed to obey the evolution law [7, 8]

$$D_{ij} = \begin{cases} 0, & \sigma_{ij} \leqslant \sigma^{\mathrm{s}}_{\mathrm{threshold}} \text{ or } \max(\sigma_i) > 0, & i \neq j \\ \dfrac{\sigma_{ij} - \sigma^{\mathrm{s}}_{\mathrm{threshold}}}{\sigma^{\mathrm{s}}_{\mathrm{crit}} - \sigma^{\mathrm{s}}_{\mathrm{threshold}}}, & \sigma^{\mathrm{s}}_{\mathrm{threshold}} < \sigma_{ij} < \sigma^{\mathrm{s}}_{\mathrm{crit}} \text{ and } \max(\sigma_i) < 0, & i = 1, 2, 3 \\ 1, & \sigma_{ij} \geqslant \sigma^{\mathrm{s}}_{\mathrm{crit}} \text{ and } \max(\sigma_i) < 0, & j = 1, 2, 3 \end{cases} \tag{5}$$

The critical stress value under impact conditions were determined to be 600 MPa in reference [8] by comparing the predicted results with experimental observations from stair-stepping tests. In reference [8], the threshold stress value of 540 MPa was used on the basis of the binary damage behaviour of the monolithic glass layers tested. In this study, a reduced threshold stress value of 300 MPa is used in order to improve convergence of the analyses and also to obtain clearer quantitative comparisons of damage magnitudes for various windshield designs. The values of $\sigma^{\mathrm{s}}_{\mathrm{crit}}$ and $\sigma^{\mathrm{s}}_{\mathrm{threshold}}$ in equation (5) are assumed to be the same as those in equation (4) for convenience [7, 8]. The influence of different values of critical and threshold stresses on the predicted damage patterns was discussed by Sun and Khaleel [7, 8]. The above-described constitutive relation is coded with FORTRAN user subroutine VUMAT.f to interface with the main ABAQUS EXPLICIT code [9].

The PVB layer is a viscoelastic polymer modelled as a so-called standard linear solid. Many polymers follow this linear viscoelastic law especially when strains are small [10]. In the finite element analysis, the PVB layer is modelled by linear viscoelastic model with only one term in the Prony series according to

$$G(t) = G_\infty + (G_0 - G_\infty)\,\mathrm{e}^{-\beta t}$$

where $G_\infty = 0.69$ MPa, $G_0 = 1.0$ GPa, and $\beta = 12.6\ \mathrm{s}^{-1}$. The bulk modulus of PVB is 2.0 GPa, Poisson's ratio is assumed to be 0.45, and the density $\rho = 1100\ \mathrm{kg/m^3}$ [5, 6].

3 EFFECTS OF DIFFERENT WINDSHIELD DESIGNS

The above-described constitutive models and analysis procedures are validated and calibrated in reference [8] with experimental data obtained for monolithic glass. In this study, the effects of different windshield designs on crack patterns and damage magnitudes are examined. The design factors considered include different glass ply thicknesses and different windshield curvatures.

3.1 Effects of glass layer thickness

In this section, flat windshields of four different thickness combinations are studied and compared. The initial normal impact velocity of the steel ball is set to be 26.82 m/s (about 60 mile/h). The purpose is to study the effects of glass ply thickness distribution on the stone-impact resistance of the windshields and to draw quantitative conclusions as to the advantage and disadvantage of using asymmetric lamination, and the possibilities for windshield weight reduction without compromising impact resistance. The four windshields studied have a common PVB layer thickness of 0.7 mm, and the thicknesses of the inner and outer glass layers are summarized in Table 1.

Since case 1 represents the typical symmetric windshield construction, it is used as the baseline for comparison. Cases 2 is also a case with symmetric construction, but both glass layers in case 2 are 0.5 mm thinner than those in case 1. Cases 3 and 4 have the same total thicknesses and are both of asymmetric construction; case 3 has a thicker outer layer and case 4 has a thicker inner layer. Compared with the baseline case, cases 2 and 3 represent 19 per cent and 10 per cent weight reduction respectively.

Table 1 Summary of ply thickness distribution of the four windshields studied

Case	Outer layer (mm)	PVB layer (mm)	Inner layer (mm)	Total thickness (mm)
1	2.3	0.7	2.3	5.3
2	1.8	0.7	1.8	4.3
3	2.3	0.7	1.8	4.8
4	1.8	0.7	2.3	4.8

Since CDM is used to model the irreversible cracking damage process of the windshield upon impact, the tendency for different cracking mechanism is interpreted through the magnitude of different components of the damage tensor. For example, Fig. 2 shows the contour plot of damage component D_{11} for case 1 at 6 μs. Since this damage component is caused by stresses in the radial direction, it represents the tendency for circular web-shaped cracking damage. The results in Fig. 2 show that most web-shaped damage occurs on surface 2 right underneath

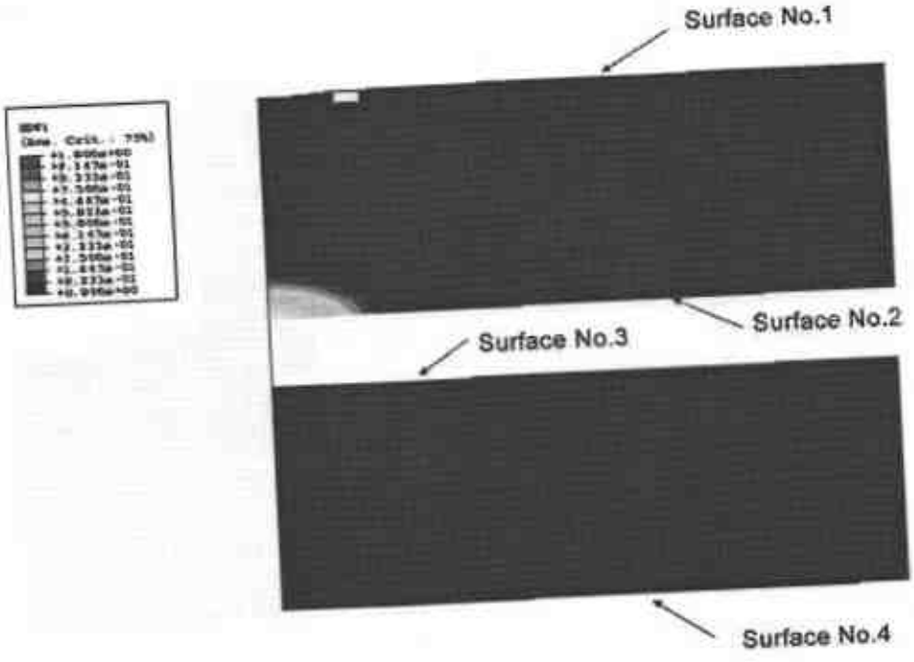

Fig. 2 D_{11} contour for case 1 at 6 μs

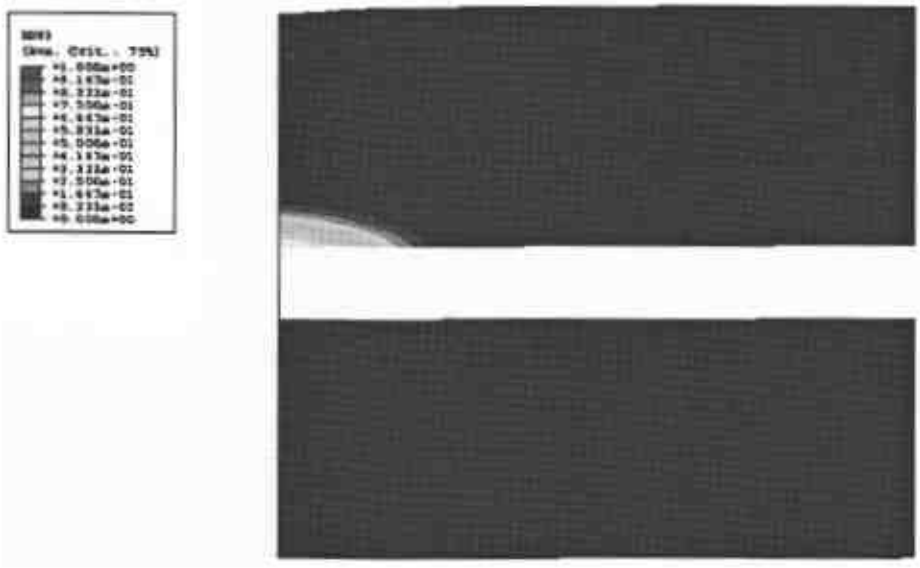

Fig. 3 D_{33} contour for case 1 at 6 μs

the impact point during the loading cycle. This is because surface 2 experiences the highest magnitude of bending-induced radial stress during impact.

Next, the contour plot of damage component D_{33} is shown in Fig. 3 for case 1. Again, surface 2 has the highest D_{33}. Because of the axisymmetric nature of the model, circumferential damage is caused by stress component σ_{33} and it represents star-shaped cracking for the impacted windshield. Comparing Figs 2 and 3, it is also clear that D_{33} has a larger damaged zone radius than D_{11} on surface 2. This prediction is consistent with most experimental impact observations in which the star-shaped cracks occur in larger areas than the web-shaped cracks (see, for examples, Fig. 4 of reference [11] and Fig. 31 of reference [12]. It is also consistent with observations from most stone-impacted in-service windshields. Also note that no damage is predicted on surfaces 3 and 4 under this impact loading condition. It should be mentioned that the results shown in Figs 2 and 3 are for case 1 at 6 μs during the loading cycle and they do not include any damage caused by crack propagation upon unloading.

In addition to the damage location on surface 2, a ring of damaged zone on surface 1 is also predicted around $r = 0.98$ mm. Since D_{11} on surface 1 corresponds to web-shaped damage, the predicted ring of damaged elements represents the possible initiation site for a Hertzian cone crack. At 6 μs, all the predicted values of D_{11} and D_{33} are below 1.0, indicating that no visible damage is predicted at this time. The predicted ring with high D_{11} value on surface 1 represents a zone degraded by the impact loading and it serves as the most probable initiation site for a Hertzian cone crack to form. Note also that no star-shaped damage, D_{33}, is predicted on surface 1.

The predicted damage components on surfaces 1 and 2 are compared next for the four cases at the end of the impact analyses when local material failure occurs. The results are illustrated in Figs 4 to 6. It should be mentioned that because of the differences in total thickness of the laminates, the times to failure for the four cases are different. For all four cases analysed, numerical problems were experienced after the onset of local material point failure on surface 2 because of damage-induced severe element distortions (Fig. 7). The data for the line plots in Figs 4 to 6 are taken at the last successful increments of the analyses for the four cases.

For all the cases considered, no damage is predicted on surfaces 3 and 4. In addition, no star-shaped damage, D_{33}, is predicted on surface 1.

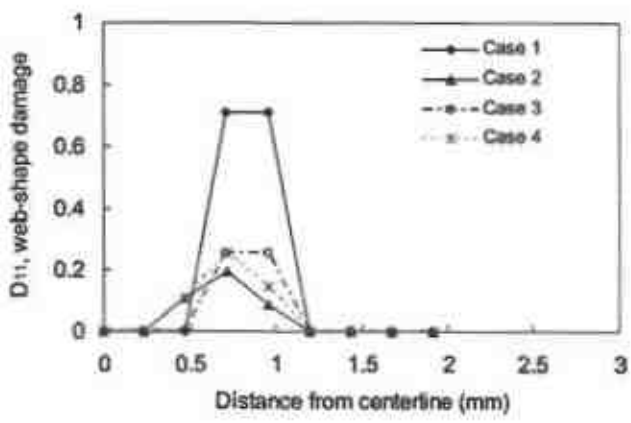

Fig. 4 Comparison of D_{11} upon impact on surface 1 for the four cases

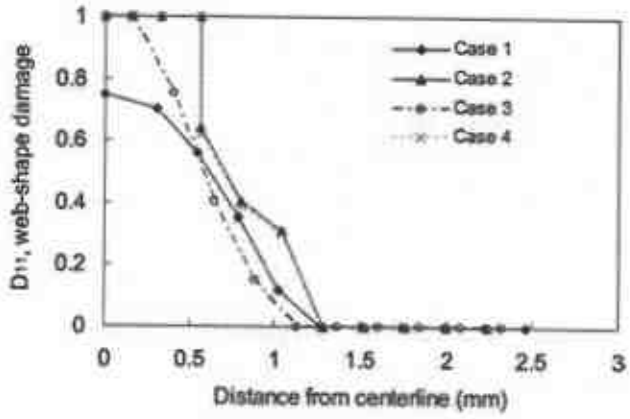

Fig. 5 Comparison of D_{11} upon impact on surface 2 for the four cases

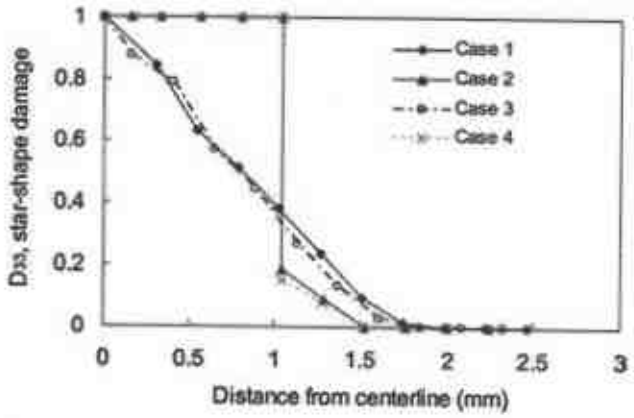

Fig. 6 Comparison of D_{33} upon impact on surface 2 for the four cases

Figure 4 compares the predicted damage component D_{11} on surface 1 for the four cases at the end of the analyses. The results suggest that the magnitude of D_{11} on surface 1 increases with increasing total thickness of the laminated glass ply. Since D_{11} on surface 1 corresponds to a Hertzian cone crack, these results indicate that a Hertzian cone crack is more likely to be the dominant cracking mechanism in thicker glass plies than in thinner glass plies. In fact, most of the experimental studies on Hertzian cone crack formation in the literature were conducted on semi-infinite glass blocks [1–4]. With reduced glass layer thickness, the bending rigidity of the cross-section is significantly reduced. Consequently, bending-induced damage would be more prominent for thinner windshields.

Figures 5 and 6 compare the values of damage components D_{11} and D_{33} on surface 2. With the outer layer thickness being the same, cases 1 and 3 have almost the same damage magnitudes D_{33} on surface 2. No visible web-shaped damage, D_{11}, is predicted for case 1, and a very small region of web-shaped crack is predicted for case 3 on surface 2. Similar conclusions for damage magnitudes on surface 2 can be made for cases 2 and 4 with the same thinner outer layer thicknesses. The predicted damage values for case 4 are only slightly lower than those of case 2. From these results, it can be concluded that the damage level on surface 2 primarily depends on the thickness of the outer glass ply. It is also evident, for all the four cases studied, that D_{33} has a larger radius than D_{11} on surface 2.

Figure 7 compares the contours of D_{12} (damage caused by maximum shear stress) on the deformed shapes for the last successful increments of the four analyses. Again, with thicker outer glass layers, Cases 1 and 3 have lower magnitudes of D_{12} than cases 2 and 4 do on surface 2. Note that, because of the severe local glass damage on surface 2, numerical problems were experienced at the end of the analyses. However, since the results presented here are for the last successful increments, they are still valid solutions. The numerical problems should not influence the conclusions obtained from these results.

With the above quantitative comparisons of radial, circumferential, and Hertzian cone damage for the four cases, some observations regarding the optimal windshield design can be made. Firstly, the outer glass layer appears to be most critical in determining the magnitude of bending-induced damage on surface 2. Less severe radial and circumferential damage on surface 2 can be achieved by increasing the outer layer thickness. Secondly, regarding the asymmetric construction, case 3 outperforms case 4 in impact resistance with the outer layer being thicker than the inner layer. Finally, by comparing cases 1 and 3, it can be concluded that case 3 achieves a weight saving of about 10 per cent without sacrificing much of its impact resistance in terms of radial and circumferential damage. Similar results were reported by the present authors and co-workers [13] using a relatively simple damage evolution law. In fact, stone-impact tests and dart tests performed by various researchers have also experimentally demonstrated the advantages of asymmetrical windshield constructions [14–16]. For example, Grant *et al.* [16] reported that impact tests using granite projectiles on laminated glass 'have shown that the critical velocity for damage initiation depends strongly on the thickness of the outermost layer of glass whereas the inner thickness has a secondary effect on this damage threshold'. This study offered more mechanics-based explanations for the above experimental observations and it also provided a simulation methodology for quantifying the influence of

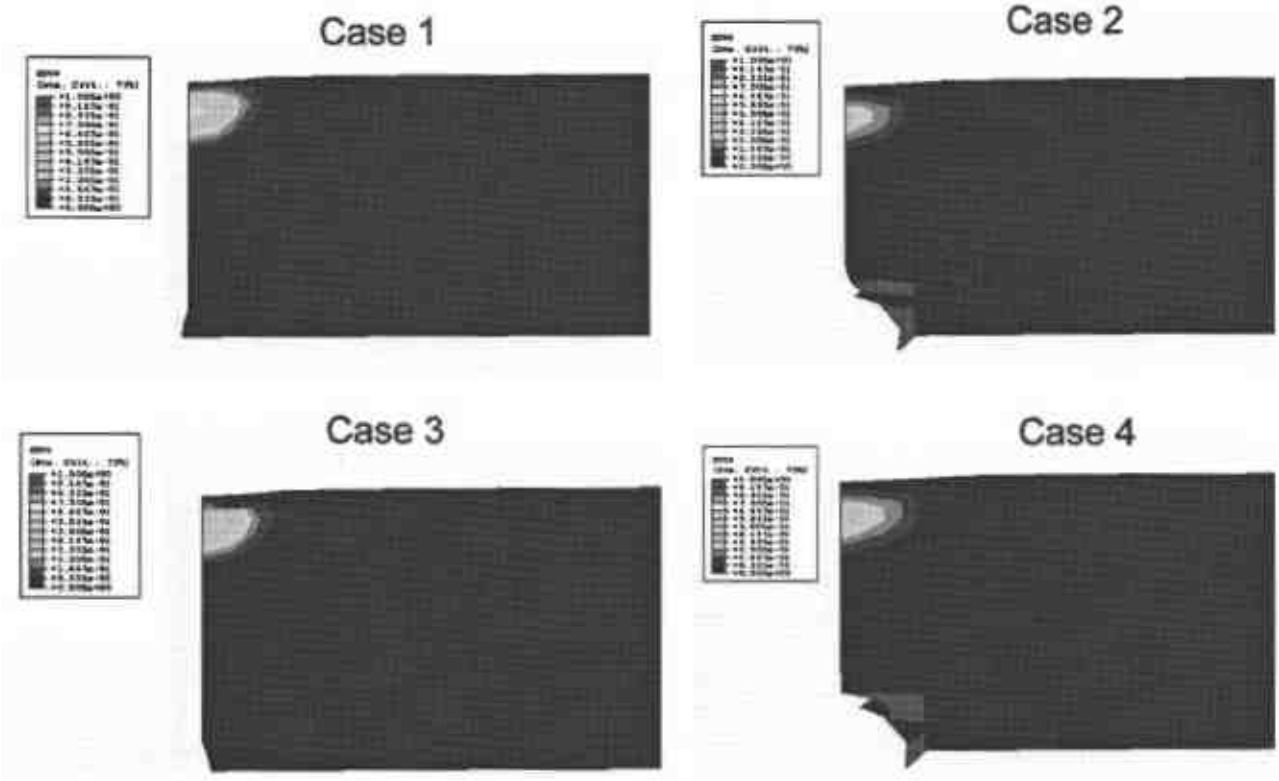

Fig. 7 D_{12} contour for all four cases at the end of the analyses

different windshield thickness combinations on its stone-impact resistance.

It is also interesting to note that, even though no visible Hertzian cone crack is predicted on surface 1 for all the cases considered, a Hertzian cone crack is more likely to be the dominant cracking mechanism for thicker laminated glass plies than for thinner glass plies. Since a Hertzian cone crack has a stable through-thickness propagation direction and it can be stopped at the glass–PVB interface, it should not be considered as severe as the radial cracks which can experience unstable in-plane propagation upon further loading and unloading.

3.2 Effects of windshield curvatures

In considering the windshield curvature effects on stone-impact resistance, laminated glass layers with three different curvatures are considered. They are a flat windshield, a curved windshield with 3 in radius, and a curved windshield with 8 in radius. For all the three cases, the thicknesses of both glass layers are kept at 2.3 mm and the thickness of the PVB layer is 0.7 mm. The initial impact velocity of the steel ball is again set to be 26.82 m/s. Only normal impact is considered.

Figure 8 shows the comparison of D_{11} on surface 1 for the three windshields. Since D_{11} on surface 1

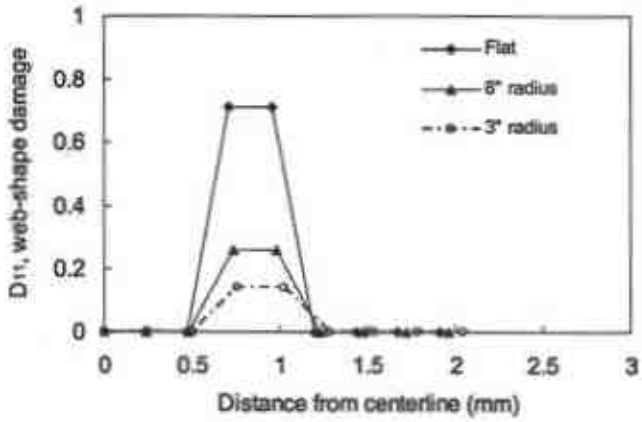

Fig. 8 Comparison of D_{11} on surface 1 for windshields with three curvatures

corresponds to the possible Hertzian cone crack, the results in Fig. 8 suggest that, with decreasing windshield curvature (increasing radius), the likelihood of Hertzian cone initiation on surface 1 increases. Figures 9 and 10 compare D_{11} and D_{33} on surface 2 for the three curvatures. Again, it is shown that the flat windshield has the highest damage values for both D_{11} and D_{33}. If a flat windshield is considered to be of infinite radius, then radial and circumferential damage decrease with decrease in the windshield radius. This is because radial damage is

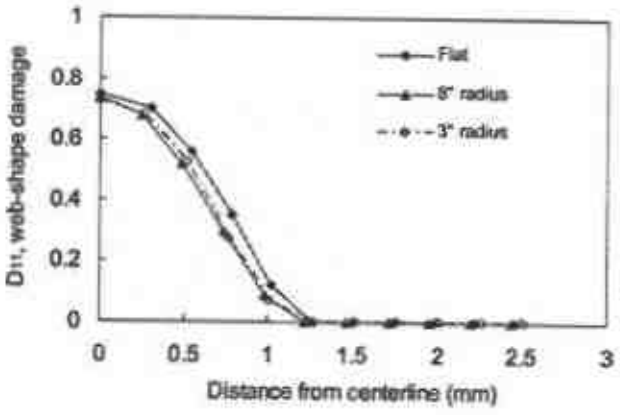

Fig. 9 Comparison of D_{11} on surface 2 for windshields with three curvatures

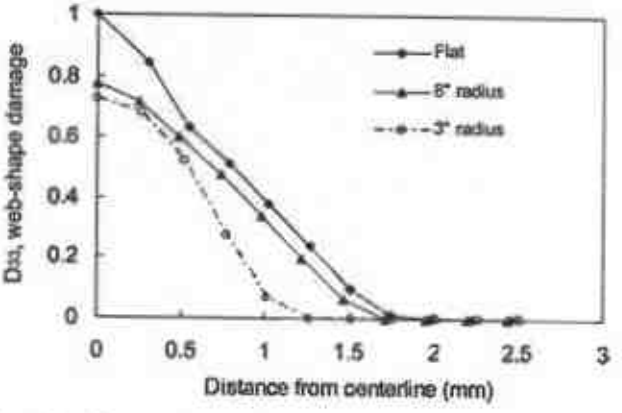

Fig. 10 Comparison of D_{33} on surface 2 for windshields with three curvatures

primarily induced by the tensile stress generated as a result of outer glass ply bending. By decreasing the glass layer radius, bending-induced stresses on surface 2 are reduced. In addition, no damage is predicted on surfaces 3 and 4 for all the three curvatures.

4 CONCLUSIONS AND DISCUSSION

In this study, explicit finite element analysis is used to simulate the damage pattern and magnitude of automotive windshields subject to the normal impact loading of a flying object. The glass layers are modelled with the CDM model with linear damage evolution and the PVB layer is modelled with a linear viscoelastic solid. In contrast with some earlier studies where the propagation rate and inclination angle of the Hertzian cone have to be prespecified, this study predicts the initiation possibilities of Hertzian cone and other damage mechanisms through interpreting different damage components on different glass surfaces upon impact loading.

The model is used to study the effects of windshield designs in terms of variations in windshield thickness and curvature on its stone-impact resistance. It is found that the thickness of the outer glass layer dominates the impact resistance of the windshield in terms of radial and circumferential cracking damage. This is consistent with many experimental results reported in the open literature. Among the four cases studied, the optimal design is found to be the case with 10 per cent weight savings and with the outer layer being 0.5 mm thicker than the inner layer of glass. It is also found that, the thicker the total laminated glass, the more likely it is that a Hertzian cone crack will form on surface 1. In addition, the higher the windshield curvature (smaller radius), the less severe are the radial damage and circumferential damage on surface 2, and the less likelihood there is for Hertzian cone damage to form on surface 1. These results can also be qualitatively validated by experimental observations reported in the literature.

It is interesting to note that the current impact modelling procedures predict the onset of radial and circumferential cracks during the loading cycle for thin laminated automotive windshields. This is different from the observations and predictions for a semi-infinite glass block under static indentation in which radial and circumferential cracks only occur during the unloading cycles [4, 7]. The reason for this difference is that, for thin laminated glass, bending-induced tensile stresses are highly localized on surface 2 during impact. Again, this study does not predict the damage growth upon unloading because of issues related to the loss of material and severe element distortions in the explicit finite element analyses.

It should be noted that the specific damage evolution law used here is critical for accurately predicting the damage fracture behaviour of laminated glass. The damage tensor for CDM is usually defined on the basis of some physical correlations of fracture modes with certain stress or strain components, and its evolution law often becomes phenomenologically based. As noted earlier, the damage tensor definition and its evolution law used in this study were developed by the present authors [7] for modelling a semi-infinite glass indentation process and by the present authors and a co-worker [8] for modelling monolithic glass impact resistance. The damage evolution law has been validated by experiments conducted by the present authors as well as observations reported in the open literature. The fact that the predicted effects for different windshield design parameters correlate well with reported experimental

observations also serves as validation for the damage model used.

It should be mentioned that this study is strictly based on a deterministic approach in which the strength of glass is assumed to be a known constant without statistical variation. In reality, however, the strength of glass depends on many factors such as its age and handling procedures. Therefore the strength of each individual windshield glass will have a probabilistic distribution that will affect the damage behaviour and cracking manner. The impact behaviour of an in-service windshield is a topic subjected to future studies. It is also assumed in this study that the glass layers are residual stress free before impact; i.e. the glass layers are in annealed condition. The impact resistance of heat strengthened and tempered glass should be the areas of further research.

ACKNOWLEDGEMENT

This work was supported by the Office of Industrial Technology, the US Department of Energy, under Contract DE-AC06-76RL01830.

REFERENCES

1 **Lawn, B. R.** Indentation of ceramics with spheres: a century after Hertz. *J. Am. Ceram. Soc.*, 1998, **81**(8), 1977–1994.
2 **Cook, R. F.** and **Pharr, G. M.** Direct observation and analysis of indentation cracking in glasses and ceramics. *J. Am. Ceram. Soc.*, 1990, **73**(4), 787–817.
3 **Lawn, B. R.** and **Wilshaw, R.** Review indentation fracture: principles and applications. *J. Mater. Sci.*, 1975, **10**, 1049–1081.
4 **Knight, C. G., Swain, M. V.,** and **Chaudhri, M. M.** Impact of small steel spheres on glass surfaces. *J. Mater. Sci.*, 1977, **12**, 1573–1586.
5 **Flocker, F. W.** and **Dharani, L. R.** Modeling fracture in laminated architectural glass subject to low velocity impact. *J. Mater. Sci.*, 1997, **32**, 2587–2594.
6 **Flocker, F. W.** and **Dharani, L. R.** Low velocity impact resistance of laminated architectural glass. *J. Archit. Engng*, March 1998, **4**(1), 12–17.
7 **Sun, X.** and **Khaleel, M. A.** Modeling of glass fracture damage using continuum damage mechanics – static spherical indentation. *Int. J. Damage Mechanics*, 2004, **13**(3), 263–285.
8 **Sun, X., Khaleel, M. A.,** and **Davies, R. W.** Modeling of stone-impact resistance of monolithic glass ply using continuum damage mechanics. *Int. J. Damage Mechanics*, 2005, **14**, 165–178.
9 *ABAQUS/Explicit User's Manual*, 1998 (Hibbitt, Karlsson and Sorensen, Inc.).
10 **Fung, Y. C.** *Foundations of Solid Mechanics*, 1965, pp. 20–28 (Prentice-Hall, Englewood Cliffs, New Jersey).
11 **Entwistle, K. M.** The fracture stress of float glass. *J. Mater. Sci.*, 1993, **28**, 2007–2012.
12 **Gulati, S. T., Helfinstine, J. D., Roe, T. A., Khaleel, M. A., Davies, R. W.,** and **Woods, J. L.** Biaxial strength of automotive windshields. Technical Report for the Structural Reliability of Lightweight Glazing Alternatives CRADA Project, Richland, Washington, 1999, Pacific Northwest National Laboratory.
13 **Sun, X., Khaleel, M. A., Davies, R. W.,** and **Gulati, S. T.** Effect of windshield design on high speed impact resistance. In Proceedings of the International Body Engineering Conference, 2000, paper 00IBECG-11 (Society of Automotive Engineers, Detroit, Michigan).
14 **Linnhofer, D.** and **Maurer, M.** Light weight conventional automotive glazing. *Automotive Glass Glazing*, 1997, **34**, 25–26.
15 **Linhofer, D.** and **Durkop, D.** Resistance of glazings to stone impact. In Proceedings of the AUTOTEST 96 Conference, 1996 (IEEE, Barcelona).
16 **Grant, P. V., Cantwell, W. J., McKenzie, H.,** and **Corkhill, P.** The damage threshold of laminated glass structures. *Int. J. Impact Engng*, 1998, **21**(9), 737–746.

APPENDIX

Notation

C_1, C_2	material constants for the damage mechanics model
D_{ij}	anisotropic damage tensor
E	Young's modulus
$G(t)$	stress relaxation function for poly(vinyl butyral)
$[K^{\mathrm{d}}_{ijkl}]$	stiffness matrix for the added influence of material damage
$[K^{\mathrm{e}}_{ijkl}]$	stiffness matrix of the undamaged elastic material
δ_{ij}	Kronecker delta defined as 1 if $i = j$ and as 0 if $i \neq j$
ε_{kl}	strain tensor
λ, μ	Lamé constants
ν	Poisson's ratio
ρ	density
σ_{crit}	critical stress level above which damage is 1
$\sigma_{\mathrm{threshold}}$	threshold stress level below which damage is 0
σ_{ij}	stress tensor